Journal of Porous Materials (2023) 30:965–974
https://doi.org/10.1007/s10934-022-01401-3

Effect of surfactant on electrochemical performance of Co_3O_4 electrode and its application in supercapacitor

Hanbo Zou[1] · Cuimiao Wang[1] · Zhiwei Feng[1] · Wei Yang[1] · Shengzhou Chen[1]

Accepted: 18 November 2022 / Published online: 30 November 2022

Abstract
Porous nanoflower-like Co_3O_4 material on conductive nickel foam substrate was synthesized by hydrothermal reaction combined with thermal decomposition method. The effects of surfactants on the morphology and electrochemical properties of Co_3O_4 electrodes were investigated. The Co_3O_4 electrodes modified with SDS, PVP and CTAB surfactants exhibited nano-flower, nano-rod and honeycomb array structures, respectively. Compared with PVP and CTAB, the addition of SDS surfactant can promote the connection of nanostructures in the solution-recrystallization process, provide a large activity area, and reduce the crystallinity of materials. In addition, SDS inserted into the interlayers is decomposed to form the hierarchical flower-like structure. The Co_3O_4-SDS sample displayed superior electrochemical properties. At the current density of 1 A g^{-1}, the specific capacitance of Co_3O_4-SDS was 1150 F g^{-1}. The specific capacitance retention was 74% after 5000 charge-discharge cycles at the current density of 8 A g^{-1}. The maximum energy density of the assembled Co_3O_4-SDS//AC supercapacitor reached 30 Wh kg^{-1} even though the power density was 813 W kg^{-1}. The energy density remained 9.0 Wh kg^{-1} as the power density increased to 16,200 W kg^{-1}.

Keywords Surfactant effect · Co_3O_4 · Hierarchical flower-like structure · Supercapacitor

1 Introduction

Nowadays, it is urgent to solve the energy dilemma by looking for an advanced energy storage mode. Because of the advantages of fast charging and discharging, high power density, and excellent cycling performance[1, 2], etc., supercapacitors have become promising new energy storage devices, which were classified as double-layer capacitors (EDLCs) and pseudocapacitors according to the mechanism of charge storage. The former store charges through the non-Faradaic process, whereas the latter store charges through the rapidly reversible Faradaic process[3]. The primary electrode materials for pseudocapacitance include metal hydroxide, metal oxide, etc. Co_3O_4 material with spinel structure has been extensively studied in the fields of lithium-ion batteries and supercapacitors owing to its high theoretical capacity (3560 F g^{-1}) [4]. Co_3O_4 can interact with the ions of the electrolyte, so that it shows outstanding electrochemical performance in both electrolytes and organic electrolytes[5]. It is well known that the performance of supercapacitors is influenced by the crystallinity, shape and specific surface area of the electrode. For example, the hybrid electrodes of NiO-Co_3O_4/graphene oxide composites provide high surface area, and the graphene sheets in the electrodes not only increase the surface area and the conductivity [6]. The in situ synthesis of heterogeneous structures grown on MXene substrates is proved to be effective in preventing the restacking of nanosheets and shortening the ion migration distance[7].

Recently many researchers have focused on nanoscale Co_3O_4 materials with different morphologies, which possess a high active surface area, the short pathway for electron and ion transfer, etc[8–10]. Wang et al. synthesized Co_3O_4 nanowire materials by reduction, and the obtained materials have the large specific surface area and provide abundant active sites for redox reactions[11]. Hoa LT et al. have synthesized Co_3O_4 with flower-like structure by one-pot hydrothermal method[12], which were assembled by 3D layered

✉ Wei Yang
wyang@gzhu.edu.cn

✉ Shengzhou Chen
szchen@gzhu.edu.cn

[1] School of Chemistry and Chemical Engineering, Guangzhou University, 510006 Guangzhou, Guangdong, China

nanosheets with mesoporous structure. High porosity and fast penetration of the Co_3O_4 electrolytes increase effectively the kinetic rate and facilitated the charge transfer.

It is well known that the addition of surfactants during the preparation process can regulate the microstructure and surface topography of materials effectively[13, 14]. The different morphologies and pore structures will affect electrochemical performance. Ail et al. prepare Sn-doped Co_3O_4 nanorods with the surfactant of PVP. In order to obtain the optimal sample morphology, the degree of PVP decomposition is changed by varying the calcination temperatures[15]. Babu R S et al. synthesized copper-cobalt oxide nanosheets with the hydrothermal synthesis. The surfactant of PVP was used as the morphology control agent, and the obtained porous nanosheet structure exposed a significant number of active sites with uninterrupted electron transfer[16]. Rajeshkhanna G et al. synthesized nested cobalt oxide nanowires by SDS and performed the good electrochemical stability due to the unique pore structure of the material[17]. Xu, YJ et al. prepared $NiCo_2O_4$/GO by co-precipitation method with the assistance of SDS simultaneously. This method took advantage of the longer molecular chain of surfactant SDS, which can reduce the surface tension of the particles and prevent the solute aggregation[18]. Amirtharaj S N et al. obtained the rod-shaped Mn_2O_3 sample adjusted with CTAB surfactant, and the specific capacitance of Mn_2O_3 was 647 F g^{-1} at the current density of 1 A g^{-1}[19]. Another way to enhance charge storage in capacitors is to avoid using binders or external carbon sources to fabricate electrodes, since the layered three-dimensional structure provides a large active surface allowing for rapid electron transfer. C Y Du et al. grew the $ZnCo_2O_4$ electrode material directly on a conductive substrate, avoiding the conductive agent and binder forming an inactive surface during the typical paste pressing process and enhancing the interface contact between the active material and the collector[20].

In this paper, porous Co_3O_4 nanoparticles on the nickel foam subtract were grown in situ by hydrothermal and thermal decomposition methods. Different Co_3O_4 electrodes were obtained by altering the types of surfactants. The effects of surfactants on the morphology and electrochemical performance of Co_3O_4 were analyzed by XRD, SEM and electrochemical performance tests. To study the actual applications of Co_3O_4, the all-solid-state ASC device was assembled with the Co_3O_4 electrode material as the positive electrode, AC electrode as the negative electrode, and PVA/KOH as the gel electrolyte, respectively.

2 Experimental

2.1 Preparation of Co_3O_4 nanomaterials

1.45 g of cobalt nitrate hexahydrate (Co $(NO)_3$•$6H_2O$) and 1.0 g of surfactant (SDS, PVP or CTAB) were dissolved in 40mL methanol solution, and stirred until the solution was uniform. A piece of NF (3 cm×5 cm) was immersed in the above solution, then transferred to the Teflon autoclave and reacted at 180℃ for 10 h. After the reaction, the NF was removed from the reactor, washed with anhydrous ethanol and deionized water successively, and dried at 80℃ overnight. Co_3O_4 nanoparticles were obtained by calcination of the above samples in the Muffle furnace for 2 h at 400℃ (see Figure S1). The synthesized Co_3O_4 products were labeled as Co_3O_4-SDS, Co_3O_4-PVP and Co_3O_4-CTAB corresponding to different surfactants used.

2.2 Characterizations

The Co_3O_4 series products were used for examination by scanning electron microscope (SEM, JEOL JSM-7001 F, Japan) with the test voltage of 15 kV. Energy Dispersive Spectroscopy (EDS) was equipped to gain the information on the chemical composition distribution. The detailed morphological features and the structure information of the samples were acquired by the transmission electron microscope (TEM, JEOL JEM-2100 F). The lattice structure of the samples was analyzed by X-ray diffraction testing (XRD, PW3040/60) with the tube current and voltage of 20 mA and 40 kV, respectively. The elemental composition and chemical valence state on the surface of the samples were analyzed by X-ray photoelectron spectroscopy (XPS, ESCALAB 250Xi spectrometer). The specific surface area and pore information were determined by ASAP2460 surface area and porosity analyzer with nitrogen as the adsorbent at 77 K. The precursors were examined using the thermogravimetric analyzer (TGA4000) between 25 and 700 °C with the heating rate of 10 ºC/min under air atmosphere.

2.3 Electrochemical measurements

The electrochemical performance of the Co_3O_4 samples were measured in a three-electrode system on the electrochemical workstation (CHI 660D workstation, Shanghai Chenhua). The samples, platinum foil and HgO/Hg electrode were used as the working electrode, counter electrode and reference electrode, respectively. 2 M KOH aqueous solution was used as electrolyte. The Co_3O_4 on nickel foam (~ 1.33 mg cm^{-2} for all three samples) were used directly as electrodes without conductive additives and binders. Cyclic voltammetry (CV) curves and the galvanostatic

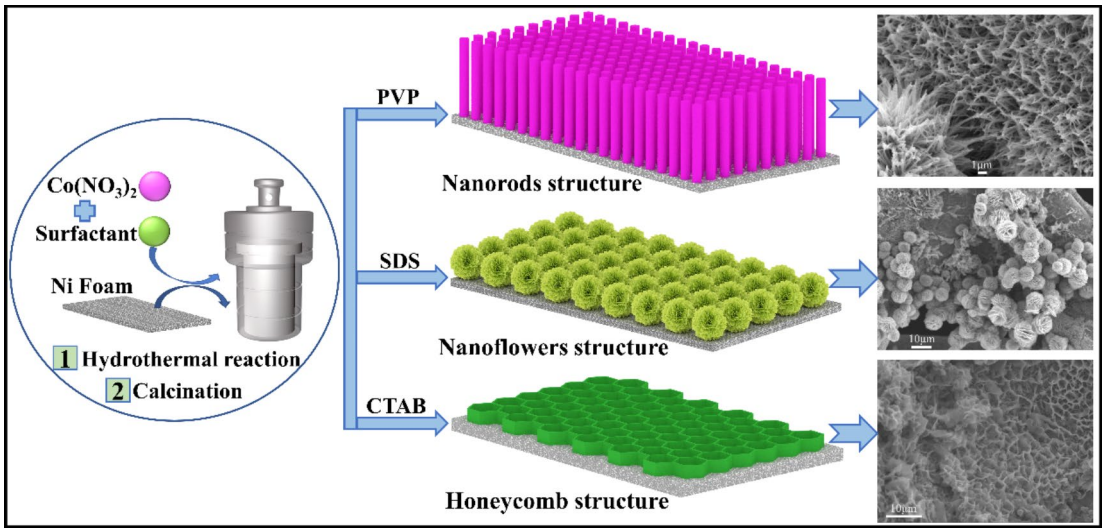

Fig. 1 Schematic illustration of the Co_3O_4 electrode with different morphologies

charge-discharge (GCD) measurements were performed at the current densities range of 1–20 A g^{-1} with the voltage between 0 and 0.6 V, respectively. Furthermore, electrochemical impedance spectroscopy (EIS) analyses were tested in the frequency range of 100 kHz to 0.01 Hz.

The specific capacitance C of the electrode material is calculated by Formula (1).

$$C = \frac{I \times \Delta t}{m \times \Delta V} \tag{1}$$

Where C is the mass capacitance of the electrode (F g^{-1}), I is the discharge current(A), Δt is the discharge time (s), m is the mass of the active substance (g), ΔV is the voltage window of the electrode (V).

An all-solid-state asymmetric supercapacitor (SC) device was assembled with Co_3O_4-SDS electrode and activated carbon (AC) electrode as positive and negative electrodes, respectively, and PVA/KOH as the gel electrolyte. According to Formula (2), the best mass ratio of anode and cathode materials of SC devices can be obtained:

$$\frac{m_-}{m_+} = \frac{\Delta V_+ C_+}{\Delta V_- C_-} \tag{2}$$

Where ΔV_+ and ΔV_- are the positive and negative voltage ranges (V), C_+ and C_- are the positive and negative specific capacities (F g^{-1}), m_+ and m_- are the masses of the positive and negative poles(g), respectively.

The energy density (E, Wh kg^{-1}) and power density (P, W kg^{-1}) of SC devices can be calculated by Formulas (3) and (4):

$$E = \frac{0.5 \times C_m \times \Delta V^2}{3.6} \tag{3}$$

$$P = \frac{E \times 3600}{\Delta t} \tag{4}$$

Where C_m,Δt and ΔV are the mass capacitance of the SC device (F g^{-1}), the discharge time (s) and the voltage window of the electrode (V), respectively.

3 Results and discussion

3.1 Characterization of structure and morphology

PVP, SDS and CTAB belong to non-ionic, anionic and cationic surfactants, respectively. By adding the three different surfactants, Co_3O_4 materials with various morphologies can be successfully grown on NF subtract. The schematic diagram and SEM patterns of Co_3O_4 samples are presented in Figs. 1 and 2, respectively. A uniform high-density Co_3O_4 nanorod array can be obtained by using PVP as the surfactant. This is because that PVP can coordinate with metal ions via the -N and C = O functional groups on the pyrrolidone ring and guide the anisotropic growth of particles[8]. During the dissolution and recrystallization processes, SDS surfactant can promote the assembly of nanostructures[21],and obtain the 3D porous high-density Co_3O_4 nanoflowers with a diameter of about 4 μm. The surfactant CTAB is able to ionize completely and produces a significant amount of CTA^+ ions, which are electrostatically attracted to the surface of Co_3O_4 particles and form a dense dual-layer protective film. Due to the repulsion of the above-mentioned film, the agglomeration of nucleated grains in the solution is decreased to some

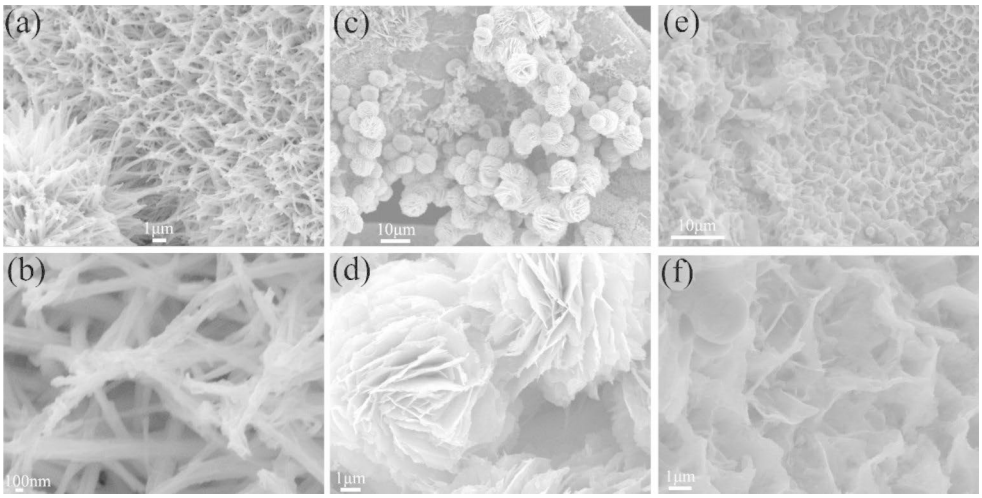

Fig. 2 SEM patterns with the low and high magnifications of Co_3O_4-PVP (a, b), Co_3O_4-SDS (c, d) and Co_3O_4-CTAB (e, f) samples

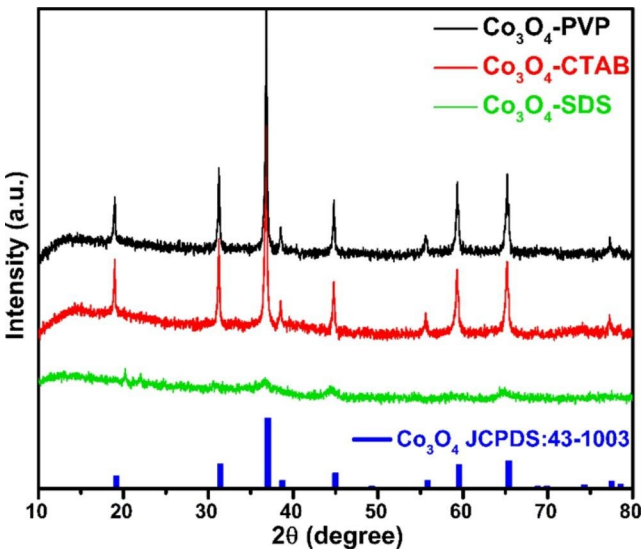

Fig. 3 XRD patterns of Co_3O_4 prepared with different surfactants

extent. Many flakes with the thickness of some nanometers can link to each other and form the honeycomb.

Figure 3 displays the XRD patterns of Co_3O_4 samples prepared with different surfactants. The peaks at 19.69°, 31.27°, 36.85°, 44.81°, 59.35° and 65.23° are assigned to the diffraction peaks of the (111), (220), (311), (400), (511) and (440) planes of cubic Co_3O_4(JCPDS No. 43-1003)[9, 10]. The XRD patterns of the three Co_3O_4 samples showed similar diffraction features and no other undesired peaks were found, indicating that the addition of surfactant did not affect the formation of Co_3O_4 crystal. Noteworthy, the diffraction peak intensity of Co_3O_4-SDS is significantly weaker than that of the other two Co_3O_4 samples. It may be due to the interaction between surfactant SDS and Co^{2+} ions, resulting in the decrease of crystallinity or the loss of some lattice planes of the synthesized Co_3O_4 product, which will be conducive to the ion transfer of the charge-discharge process[18].

The isothermal adsorption and desorption experiment of N_2 was used to obtain the specific surface and pore size distribution of Co_3O_4 samples, as shown in Fig. 4. The three Co_3O_4 samples showed the characteristics of type IV adsorption isotherms, confirming the existence of mesoporous structures[22, 23]. The surfactants selectively adsorb on specific crystal planes of Co_3O_4 crystalline nucleuses and form the mesoporous structures due to the decomposition of surfactant during the calcination[24]. The calculated specific surface area of Co_3O_4-SDS is 44.8 $m^2\ g^{-1}$, larger than that of Co_3O_4-PVP (36.2 $m^2\ g^{-1}$) and Co_3O_4-CTAB (17.5 $m^2\ g^{-1}$), respectively. Based on IUPAC categories, the

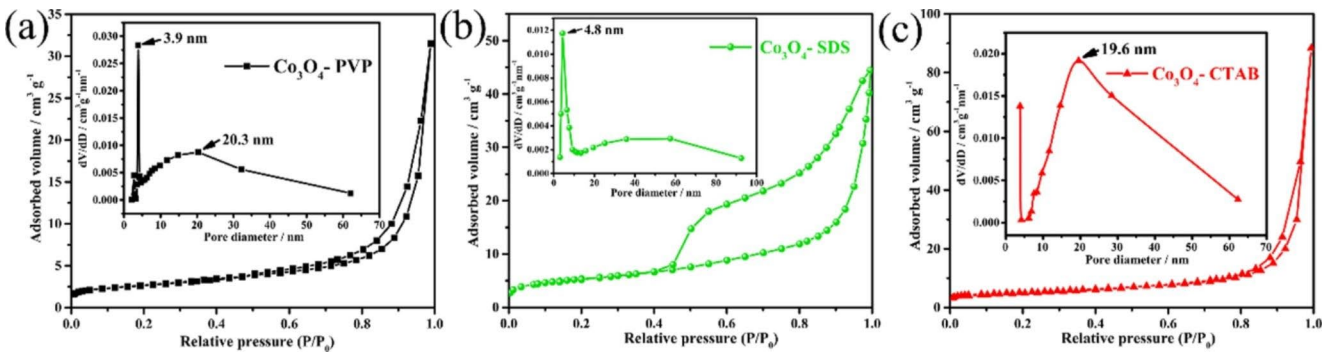

Fig. 4 N_2 adsorption-desorption curves and BJH pore size distributions(inset) of Co_3O_4-PVP (a), Co_3O_4-SDS (b) and Co_3O_4-CTAB (c)

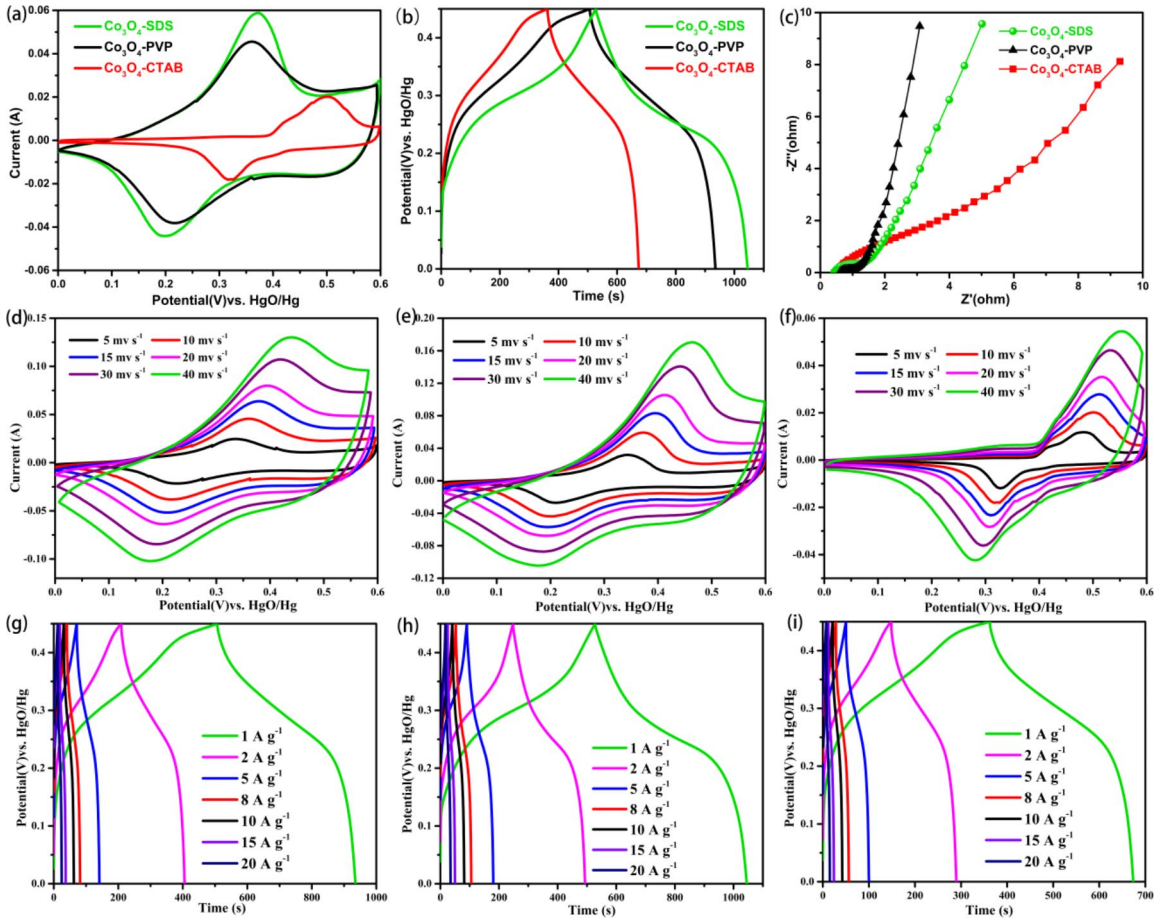

Fig. 5 (a) CVs, (b) GCDs and (c) EISs, (d-f) CVs at varying latent scanning rates and (g-i) GCDs at different current densities of Co_3O_4-PVP, Co_3O_4-SDS and Co_3O_4-CTAB electrode

adsorption and desorption isotherms of Co_3O_4-SDS materials show an H3-type hysteresis ring, indicating the existence of slat-like holes in the material. The pore diameter profiles of the samples were obtained using the BJH method. It was found that the pore size were mostly concentrated in the range of 2-20 nm (Fig. 4). In contrast, Co_3O_4-SDS material had a larger specific area and more uniform pore size than other Co_3O_4 samples. This is because the negatively charged dodecyl group in SDS can easily be attracted by Co^{2+} ions through electrostatic action, thus a large amount of SDS surfactants are inserted into the interlayer and form the hierarchical porous flower structure during the calcination[21]. At the same time, SDS can be decomposed completely below 400°C, but the thermal decomposition temperature of PVP is higher than 400°C. Fewer pores of the Co_3O_4-SDS were blocked compared with those of Co_3O_4-PVP particles[25]. Therefore, both internal and external surfaces of flower-like Co_3O_4-SDS can be fully utilized for charge transfer. The electrochemical reaction sites are greatly increased, thus Co_3O_4-SDS can offer the great surface of contact area between the active material and the electrolyte, which facilitates electrolyte penetration, ions and electrons transfer, etc.

3.2 Electrochemical characterization of Co_3O_4 electrodes

The electrochemical properties of Co_3O_4 series single electrodes are shown in Fig. 5. It can be seen that the CV curves of the three Co_3O_4 electrodes all have a pair of redox peaks, suggesting that their capacitive characteristics are mainly through the Faradaic reaction. The charge-storage mechanism of the Co_3O_4 electrode in KOH solution is as following processes [26].

$$Co_3O_4 + OH^- + H_2O \Leftrightarrow 3CoOOH + e^- \quad (5)$$

$$CoOOH + OH^- \Leftrightarrow CoO_2 + H_2O + e^- \quad (6)$$

Compared with Co_3O_4-PVP and Co_3O_4-CTAB electrodes, the CV curve of the Co_3O_4-SDS electrode has a higher redox

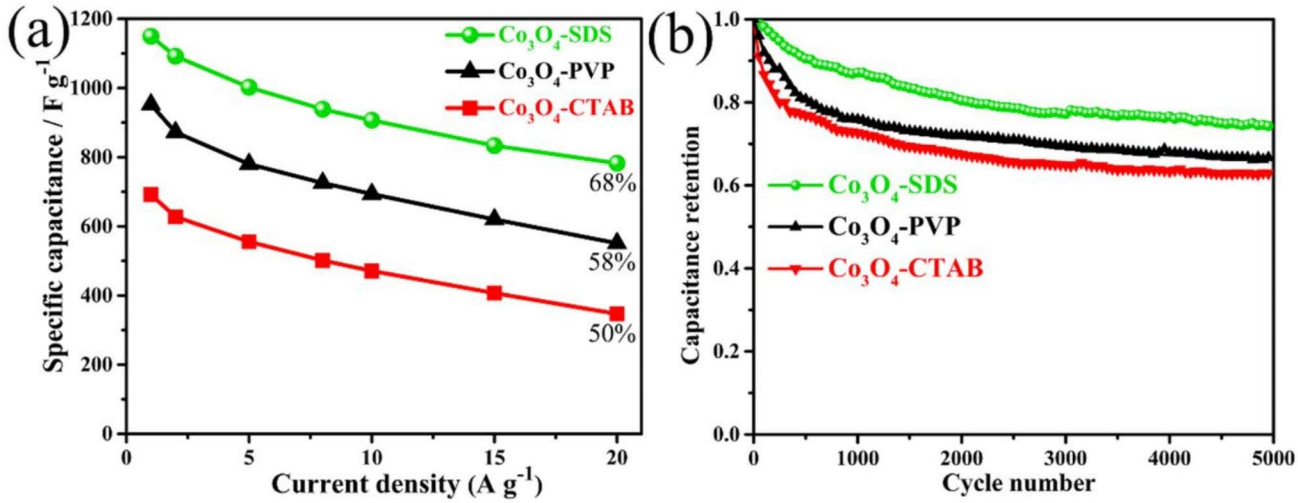

Fig. 6 Rate capabilities (a) and cycling performance (b) of Co_3O_4-PVP, Co_3O_4-SDS and Co_3O_4-CTAB electrodes

peak and a larger closed area, indicating that Co_3O_4 material with the three-dimensional nanoflower structure has good electrochemical performance. GCD test results showed that the charge/discharge profiles of the three samples had prominent potential platforms. The specific capacitance of the Co_3O_4-SDS electrode is 1150 F g^{-1}, which is superior to that of Co_3O_4-PVP (952 F g^{-1}) and Co_3O_4-CTAB (692 F g^{-1}). This is due to the nanoflower arrays of Co_3O_4-SDS with the advantages of the large specific area and porous characteristics, which contribute to the electrochemical energy storage.

Figure 5c shows the EIS curve of Co_3O_4 series electrode materials. The equivalent series resistance of Co_3O_4-SDS, Co_3O_4-PVP and Co_3O_4-CTAB electrodes are 0.43, 0.61 and 0.49Ω, respectively. The Co_3O_4-SDS electrode has the lowest total resistance among the three electrodes. Semicircle formed at the high-frequency range represents the kinetic resistance of charge transport at the electrode/electrolyte interface or the intrinsic charge transfer resistance of porous electrodes[27]. The slope in the low-frequency region is related to the Warburg impedance and associated with the electrolyte diffusion in Co_3O_4[9, 28]. The semicircle diameter of the Co_3O_4-CTAB electrode in the high-frequency region is significantly greater than that of the other two Co_3O_4 electrodes, which means that the Co_3O_4-CTAB electrode has a significant charge transfer resistance. These results indicate that Co_3O_4-SDS and Co_3O_4-PVP electrodes performe faster charge transfer behavior than Co_3O_4-CTAB with honeycomb structure. Only the slope of Co_3O_4-SDS at low frequency is close to 1, indicating that the capacitive properties and electrolyte diffusion rate of this electrode are best. The main reason is that the electrode with a hierarchical porous structure is able to overcome the primary kinetic limits of the electrochemical process, benefit the electrolyte to penetrate easily throughout the oxide substrate and reduce further the diffusion resistance[27].

Figure 5(d-f) presents the CV profiles of three Co_3O_4 samples at different scanning rates. The specific capacitance value decreases with increasing scan rate because there is enough time for ion exchange in redox reactions at lower scan rates[29]. At a higher scanning rate of 40mV s^{-1}, no apparent electrode polarization occurs in CV curves, indicating that the three materials have good reversibility. The CV profile of the Co_3O_4-SDS electrode has the highest induced current and the largest curve-closed area among the Co_3O_4 series samples. Because the rapid insertions of a large amount of OH^- ions at the electrode/electrolyte boundary are required at higher densities of KOH electrolyte, the rate of this insertion process is controlled by the diffusion step[30]. The results of EIS show that Co_3O_4-SDS has lower Warburg impedance and faster diffusion rate, thus it exhibits the quicker OH^- ions insertion rate and higher electrochemical specific capacitance. The charge/discharge curves of the three electrodes at current densities of 1–20 A g^{-1} show the typical nonlinear behavior, which verifies that the charge and discharge processes of Co_3O_4 materials conform to the Faradaic characteristics. Under the current density of 1 A g^{-1}, the specific capacitance of Co_3O_4-SDS, Co_3O_4-PVP and Co_3O_4-CTAB electrodes are 1150, 952 and 692 F g^{-1}, respectively. Co_3O_4-SDS is able to supply plenty of active sites for Faradaic reactions due to its high surface area.

Figure 6 studies the rate performance and cycle test of Co_3O_4-PVP, Co_3O_4-SDS and Co_3O_4-CTAB electrodes. At the current density of 20 A g^{-1}, the capacitance retention of the Co_3O_4-SDS electrode is about 68%, which is better than that of the Co_3O_4-PVP electrode (58%) and Co_3O_4-CTAB electrode (50%). After 5000 cycles, the

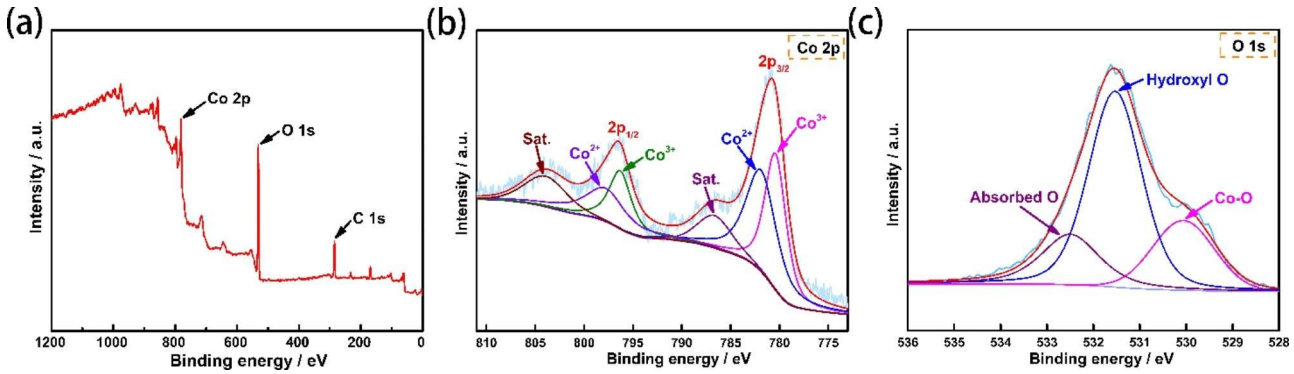

Fig. 7 (a) XPS survey spectrum, (b) Co2p and (c) O1s XPS spectra of Co_3O_4-SDS sample

Co_3O_4-SDS electrode still maintains 74% capacitance, while the capacitance retentions of the Co_3O_4-PVP electrode and Co_3O_4-CTAB electrode are 63% and 67%, respectively. This is because the petals of Co_3O_4-SDS nanoflowers expand and the spatial structure between the petals becomes closer (see Figure S4) during cycling, which can buffer the stress generated in the continuous charging and discharging process to a certain extent. The spatial confinement between the petals slows down the falling of Co_3O_4 active components during the cycles, thus Co_3O_4-SDS with nanoflower morphology shows the best cycle stability.

To further define the chemical constitution and element valence of the nano-flowered Co_3O_4 electrode, the XPS characterization analysis of different Co_3O_4 electrodes are shown in Fig. 7. For the Co 2p XPS spectrum, two peaks at the binding energies of 780.4 eV and 796.3 eV are assigned to $2p_{3/2}$ and $2p_{1/2}$ characteristic peaks of Co^{3+}, respectively. In comparison, two peaks of 781.9 eV and 797.8 eV are attributed to the distinct peaks of Co^{2+} species. The XPS results show that Co^{2+} and Co^{3+} species can coexist in Co_3O_4-SDS samples, and the redox reaction of Co_3O_4 charge storage depends on the continuous conversion between Co^{2+} and Co^{3+}[26], which can provide ultra-high Faraday activity for the Co_3O_4-SDS electrode. The XPS O1s patterns of the Co_3O_4-SDS sample are fitted to three peaks at 530.1, 531.5 and 532.5 eV, corresponding to the lattice oxygen (Co-O), surface hydroxide (Hydroxyl O) and surface pollution or oxygen vacancy, respectively[14, 31].

The structure and phase composition of Co_3O_4-SDS material was further studied by the TEM technique, as shown in Fig. 8. Co_3O_4-SDS sample show nanoflower-like particles made up of many stacked flakes. The lattice stripes of 0.207 nm, 0.286 nm and 0.245 nm are assigned to the (400), (220) and (311) crystallographic planes of cubic phase Co_3O_4, respectively[32]. The elements of Co, O and Ni are homogeneously dispersed on the surface of Co_3O_4-SDS through element surface scanning (h-j in Fig. 8) [33]. Here, the presence of Ni is due to the effect of in situ growth of the active material on nickel foam[14].

3.3 Co_3O_4//AC Electrochemical properties of asymmetric supercapacitors

Figure 9 shows the electrochemical performance of the flexible SC device assembled by Co_3O_4-SDS and AC electrodes. The CV curves of the device have no redox peak, and the charge-discharge patterns show apparent symmetry, indicating that charge balance has been reached between the electrodes of Co_3O_4//AC devices. The SC device shows excellent electrochemical characteristics at high discharge power. At the current density of 1 A g^{-1}, the specific capacitance of Co_3O_4 //AC is 83.0 F g^{-1}. Even if the current increases to 15 A g^{-1}, the specific capacitance is able to retain at 33.8 F g^{-1}.

The energy density of the SC device is calculated according to the Eqs. (3) and (4) at different power densities, as shown in Fig. 9d. When the power density is 813 W kg^{-1}, the maximum energy density is 30 Wh kg^{-1}. At the high-power density of 16,200 W kg^{-1}, the Co_3O_4//AC device still has 9.0 Wh kg^{-1} energy density. According to Table 1, the electrochemical properties of the Co_3O_4//AC device are better than those of the Co_3O_4 series supercapacitors recently reported. After 5000 cycles, the device retained 72% of its initial specific capacitance at 4 A g^{-1}, showing a remarkable cycle life (see Fig. 9e). Compared with the EIS curves of SC devices before and after stability tests (see Fig. 9f), it is found that the semi circulation diameter of the EIS curve increases significantly after the cycling, indicating higher charge transfer resistance of the Co_3O_4 electrode after cycling. The morphology and structure of Co_3O_4 cathode material changed partly after the stability test, thus the charge transfer rate of the Co_3O_4//AC capacitor decreased to some extent.

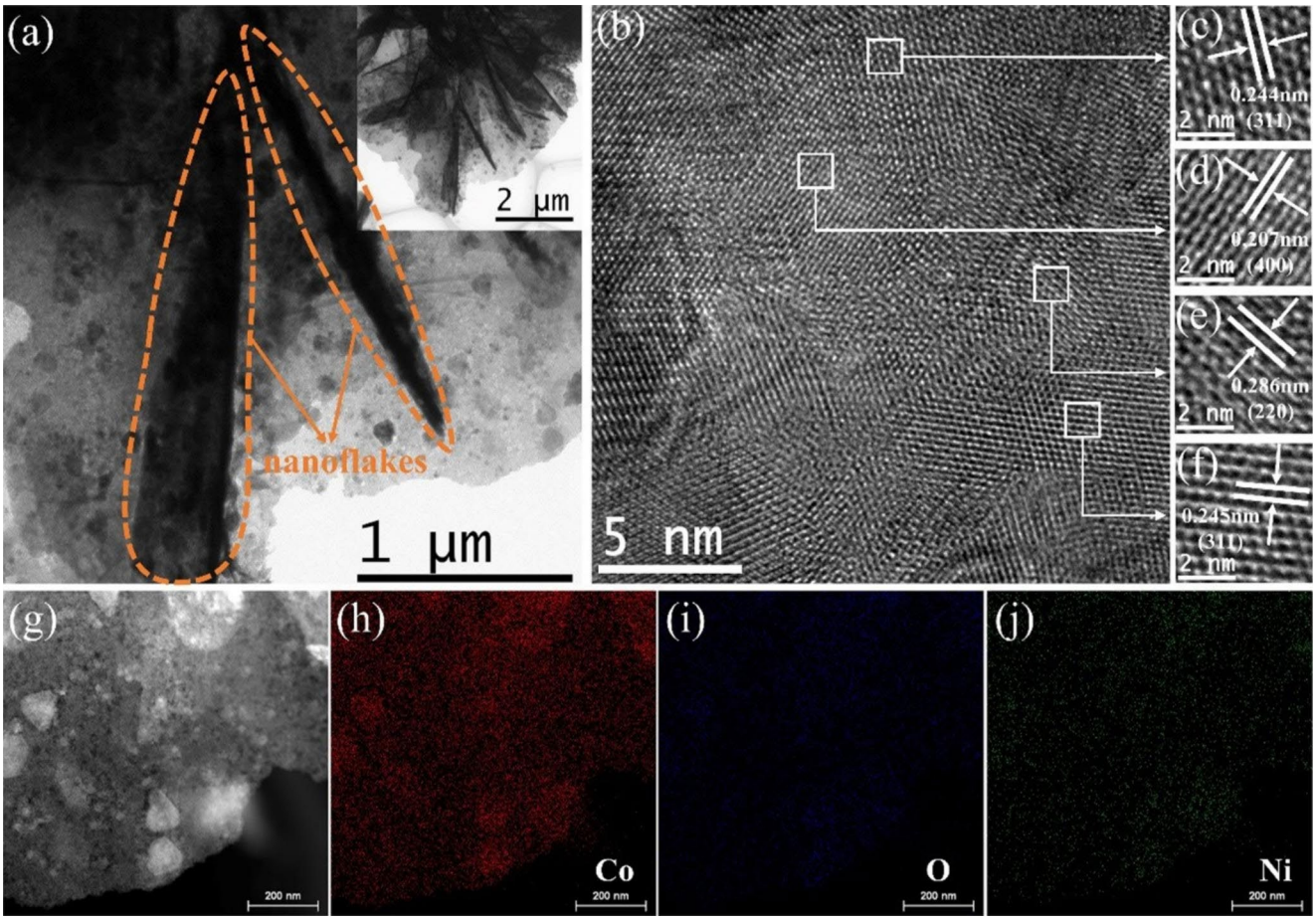

Fig. 8 (a) TEM image, (b–f) HRTEM images, (g) HAADF-STEM image, and (h–j) EDS mapping images of Co_3O_4-SDS sample

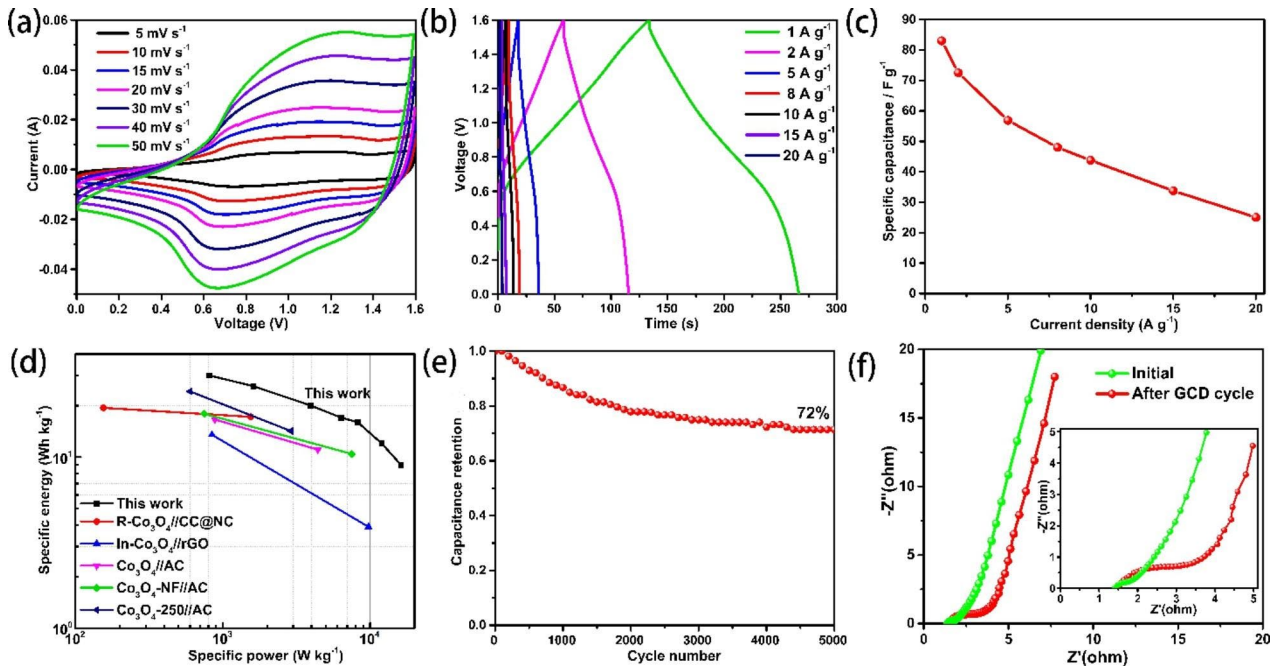

Fig. 9 (a) CV curves at different sweep speeds, (b) GCDs at various current densities, (c) specific capacitance of the Co_3O_4//AC ASC, (d) Ragone plots, (e) cycling performance evaluated at 4 A g^{-1} and (f) EISs before and after cyclic tests

Table 1 Comparison of the energy densities and power densities of various devices

Device	Energy density/ (W h kg^{-1})	Power density/ (W kg^{-1})	Ref.
R-Co_3O_4//CC@NC	17.2	1546	[34]
In-Co_3O_4//rGO	13.51	844	[35]
Co_3O_4//AC	16.6	833	[36]
Co_3O_4-NF//AC	17.9	750	[37]
Co_3O_4-250//AC	24.2	600	[38]
Co_3O_4-SDS//AC	30	813	\

4 Conclusion

Co_3O_4 porous materials were prepared in situ on conductive nickel foam substrate by hydrothermal reaction and subsequent thermal decomposition. The addition of different surfactants can effectively adjust the microstructure and surface morphology of materials. Compared with PVP and CTAB, surfactant SDS was inserted into Co_3O_4 layers through ion exchange and decomposed at high temperature, thus the Co_3O_4 sample with the hierarchical flower-like structure was synthesized. Co_3O_4-PVP and Co_3O_4-CTAB were nano rod-like arrays and honeycomb arrays, respectively. The hierarchical flower-like structure increases the active surface, slows the falling of Co_3O_4 particles from nickel foam during the cycle and favors the electrolyte permeation and ion/electron transport. The flower-like Co_3O_4-SDS electrode showed excellent electrochemical properties. At the current density of 1 A g^{-1}, the specific capacitance is 1150 F g^{-1}. During 5000 cycles under 8 A g^{-1}, 74% of the initial specific capacitance can still be preserved. The assembled Co_3O_4//AC device shows excellent rate capability with an energy density of 9.0 W h kg^{-1} even at the power density of 16,200 W kg^{-1}. The layered nanoflower-like Co_3O_4 electrode has great application potential as pseudocapacitance electrode material.

Supplementary Information The online version contains supplementary material available at https://doi.org/10.1007/s10934-022-01401-3.

Acknowledgements This work was funded by the National Natural Science Foundation of China (Grant No. 21776051), Guangzhou Science and Technology Plan Project (Grant No.202201010079) and the Natural Science Foundation of Guangdong Province (Grant No. 2022A1515011715).

Authors' contributions **Hanbo Zou**: Resources, Writing - review & editing. **Cuimiao Wang**: Conceptualization, Methodology, Formal analysis, Investigation, Writing - original draft. **Zhiwei Feng**: Data curation. **Wei Yang**: Investigation. **Shengzhou Chen**: Supervision.

Declarations

Competing interests The authors declare that they have no known competing financial interests or personal relationships that could have appeared to influence the work reported in this paper.

References

1. T.T. Ma, J.D. Chen, M. Chen, S.S. Liu, J.T. Luo, H.B. Zou, W. Yang, S.Z. Chen, Nickel -cobalt -molybdenum sulfides with adjustable morphology via coprecipitation and hydrothermal conversion as high-performance electrodes for asymmetric supercapacitors J. Alloys Compd., 838 (2020) https://doi.org/10.1016/j.jallcom.2020.155631
2. V. Gajraj, C.R. Mariappan, Electrochemical performances of asymmetric aqueous supercapacitor based on porous $Cu_3Mo_2O_9$ petals and $La_2Mo_3O_{12}$ nanoparticles fabricated through a simple co-precipitation method. Appl. Surf. Sci., 512 (2020) https://doi.org/10.1016/j.apsusc.2020.145648
3. V.T. Chebrolu, B. Balakrishnan, V. Raman, I. Cho, J.S. Bak, K. Prabakar, H.J. Kim, Co-electrodeposition of $NiCu(OH)_2$@Ni-Cu-Se hierarchical nanoparticle structure for supercapacitor application with enhanced performance. Appl. Surf. Sci., 506 (2020) https://doi.org/10.1016/j.apsusc.2019.145015
4. D.X. Guo, X.M. Song, F.B. Li, L.C. Tan, H.Y. Ma, L.L. Zhang, Y.Q. Zhao, Oriented synthesis of Co_3O_4 core-shell microspheres for high-performance asymmetric supercapacitor. Colloids And Surfaces A-Physicochemical And Engineering Aspects **546**, 1–8 (2018). https://doi.org/10.1016/j.colsurfa.2018.02.072
5. S. Vijayakumar, A.K. Ponnalagi, S. Nagamuthu, G. Muralidharan, Microwave assisted synthesis of Co_3O_4 nanoparticles for high-performance supercapacitors. Electrochim. Acta **106**, 500–505 (2013). https://doi.org/10.1016/j.electacta.2013.05.121
6. R. Lakra, R. Kumar, P.K. Sahoo, D. Thatoi, A. Soam, A mini-review: Graphene based composites for supercapacitor application. Inorg. Chem. Commun., 133 (2021) https://doi.org/10.1016/j.inoche.2021.108929
7. M.Q. Wang, X.L. Liu, B.Y. Qin, Z.Y. Li, Y.F. Zhang, W. Yang, H.S. Fan, In-situ etching and ion exchange induced 2D-2D MXene@Co_9S_8/$CoMo_2S_4$ heterostructure for superior na + storage. Chem. Eng. J., 451 (2023) https://doi.org/10.1016/j.cej.2022.138508
8. Z.Z. Zeng, L.Z. Zhu, E.S. Han, X.C. Xiao, Y.R. Yao, L.M. Sun, Soft-templating and hydrothermal synthesis of $NiCo_2O_4$ nanomaterials on ni foam for high-performance supercapacitors. Ionics **25**, 2791–2803 (2019). https://doi.org/10.1007/s11581-018-2813-y
9. D.S. Patil, S.A. Pawar, J.C. Shin, Core-shell structure of Co_3O_4@CdS for high performance electrochemical supercapacitor. Chem. Eng. J. **335**, 693–702 (2018). https://doi.org/10.1016/j.cej.2017.11.007
10. J.J. Xu, T. Xiao, X.Y. Tan, P. Xiang, L.H. Jiang, D. Wu, J. Li, S.L. Wang, A new asymmetric aqueous supercapacitor: Co_3O_4//Co_3O_4@polypyrrole. J. Alloys Compd. **706**, 351–357 (2017). https://doi.org/10.1016/j.jallcom.2017.02.253
11. Y.C. Wang, T. Zhou, K. Jiang, P.M. Da, Z. Peng, J. Tang, B.A. Kong, W.B. Cai, Z.Q. Yang, G.F. Zheng, Reduced Mesoporous Co_3O_4 nanowires as efficient Water Oxidation Electrocatalysts and Supercapacitor Electrodes. Adv. Energy Mater., 4 (2014) https://doi.org/10.1002/aenm.201400696
12. L.T. Hoa, J.S. Chung, S.H. Hur, A highly sensitive enzyme-free glucose sensor based on Co_3O_4 nanoflowers and 3D graphene oxide hydrogel fabricated via hydrothermal synthesis. Sens. Actuators B-Chemical **223**, 76–82 (2016). https://doi.org/10.1016/j.snb.2015.09.009
13. C. Sambathkumar, R. Ranjithkumar, S.E. Arasi, A. Manikandan, N. Nallamuthu, M.K. Kumar, A. Arivarasan, P. Devendran, High-performance nickel sulfide modified electrode material from single-source precursor for energy storage application. J. Mater.

Science-Materials Electron. **32**, 20058–20070 (2021). https://doi.org/10.1007/s10854-021-06383-7
14. C. Sambathkumar, N. Nallamuthu, M.K. Kumar, S. Sudhahar, P. Devendran, Electrochemical exploration of cobalt sulfide nanoparticles synthesis using cobalt diethyldithiocarbamate as single source precursor for hybrid supercapacitor device. J. Alloys Compd., 920 (2022) https://doi.org/10.1016/j.jallcom.2022.165839
15. F. Ali, N.R. Khalid, Effect of calcination temperature on structural, morphological and electrochemical properties of Sn doped Co_3O_4 nanorods. Ceram. Int. **46**, 24137–24146 (2020). https://doi.org/10.1016/j.ceramint.2020.06.193
16. R.S. Babu, R. Vinodh, A.L.F. de Barros, L.M. Samyn, K. Prasanna, M.A. Maier, C.H.F. Alves, H.J. Kim, Asymmetric supercapacitor based on carbon nanofibers as the anode and two-dimensional copper cobalt oxide nanosheets as the cathode. Chem. Eng. J. **366**, 390–403 (2019). https://doi.org/10.1016/j.cej.2019.02.108
17. G. Rajeshkhanna, E. Umeshbabu, G. Ranga Rao, Charge storage, electrocatalytic and sensing activities of nest-like nanostructured Co_3O_4. J. Colloid Interface Sci. **487**, 20–30 (2017). https://doi.org/10.1016/j.jcis.2016.10.011
18. Y.J. Xu, L.C. Wang, P.Q. Cao, C.L. Cai, Y.B. Fu, X.H. Ma, Mesoporous composite nickel cobalt oxide/graphene oxide synthesized via a template-assistant co-precipitation route as electrode material for supercapacitors. J. Power Sources **306**, 742–752 (2016). https://doi.org/10.1016/j.jpowsour.2015.12.106
19. S.N. Amirtharaj, M. Mariappan, Rapid and controllable synthesis of Mn_2O_3 nanorods via a sonochemical method for supercapacitor electrode application. Appl. Phys. A-Materials Sci. Process., 127 (2021) https://doi.org/10.1007/s00339-021-04774-5
20. C.Y. Du, E.S. Han, L.M. Sun, S.P. Qiao, L.N. Li, Template agent for assisting in the synthesis of $ZnCo_2O_4$ on ni foam for high-performance supercapacitors. Ionics **26**, 383–391 (2020). https://doi.org/10.1007/s11581-019-03189-w
21. J. Zhang, X.L. Xie, C.J. Li, H. Wang, L.J. Wang, The role of soft colloidal templates in the shape evolution of flower-like MgAl-LDH hierarchical microstructures. RSC Adv. **5**, 29757–29765 (2015). https://doi.org/10.1039/c5ra01561h
22. J.L. Lv, M. Yang, T.X. Liang, H. Miura, Facile synthesis of Co_3O_4@MnO_2 core-shell nanocomposites for high-performance supercapacitor. Mater. Lett. **197**, 127–130 (2017). https://doi.org/10.1016/j.matlet.2017.03.127
23. Y.S. Gai, Y.Y. Shang, L.Y. Gong, L.H. Su, L. Hao, F.Y. Dong, J.Z. Li, A self-template synthesis of porous $ZnCo_2O_4$ microspheres for high-performance quasi-solid-state asymmetric supercapacitors. RSC Adv. **7**, 1038–1044 (2017). https://doi.org/10.1039/c6ra25950b
24. D.U. Lee, B.J. Kim, Z.W. Chen, One-pot synthesis of a mesoporous $NiCo_2O_4$ nanoplatelet and graphene hybrid and its oxygen reduction and evolution activities as an efficient bi-functional electrocatalyst. J. Mater. Chem. A **1**, 4754–4762 (2013). https://doi.org/10.1039/c3ta01402a
25. D.-W. Wang, F. Li, M. Liu, G.Q. Lu, H.-M. Cheng, 3D aperiodic hierarchical porous graphitic carbon material for high-rate electrochemical capacitive energy storage. Angewandte Chemie-International Edition **47**, 373–376 (2008). https://doi.org/10.1002/anie.200702721
26. R. Kumar, A. Soam, V. Sahajwalla, Carbon coated cobalt oxide (CC-Co_3O_4) as electrode material for supercapacitor applications. Mater. Adv. **2**, 2918–2923 (2021). https://doi.org/10.1039/d1ma00120e
27. R. Ding, L. Qi, M.J. Jia, H.Y. Wang, Hydrothermal and soft-templating synthesis of mesoporous $NiCo_2O_4$ nanomaterials for high-performance electrochemical capacitors. J. Appl. Electrochem. **43**, 903–910 (2013). https://doi.org/10.1007/s10800-013-0580-z
28. B. Liu, D.Z. Kong, J. Zhang, Y. Wang, T.P. Chen, C.W. Cheng, H.Y. Yang, 3D hierarchical Co_3O_4@Co_3S_4 nanoarrays as cathode materials for asymmetric pseudocapacitors. J. Mater. Chem. A **4**, 3287–3296 (2016). https://doi.org/10.1039/c5ta09344a
29. C. Sambathkumar, M.K. Kumar, N. Nallamuthu, K. Rajesh, P. Devendran, Investigations on electrochemical performances of $Co(OH)_2$, Fe_2O_3 and Mn_3O_4 nanoparticles covered carbon micro spheres for supercapacitor application. Inorg. Chem. Commun., 134 (2021) https://doi.org/10.1016/j.inoche.2021.109057
30. M.W. Xu, D.D. Zhao, S.J. Bao, H.L. Li, Mesoporous amorphous MnO_2 as electrode material for supercapacitor. J. Solid State Electrochem. **11**, 1101–1107 (2007). https://doi.org/10.1007/s10008-006-0246-4
31. K. Chhetri, A.P. Tiwari, B. Dahal, G.P. Ojha, T. Mukhiya, M. Lee, T. Kim, S.H. Chae, A. Muthurasu, H.Y. Kim, A ZIF-8-derived nanoporous carbon nanocomposite wrapped with Co_3O_4-polyaniline as an efficient electrode material for an asymmetric supercapacitor. J. Electroanal. Chem., 856 (2020) https://doi.org/10.1016/j.jelechem.2019.113670
32. R. Kumar, S.M. Youssry, H.M. Soe, M.M. Abdel-Galeil, G. Kawamura, A. Matsuda, Honeycomb-like open-edged reduced-graphene-oxide-enclosed transition metal oxides (NiO/Co_3O_4) as improved electrode materials for high-performance supercapacitor. J. Energy Storage, 30 (2020) https://doi.org/10.1016/j.est.2020.101539
33. K. Seevakan, A. Manikandan, P. Devendran, A. Baykal, T. Alagesan, Electrochemical and magneto-optical properties of cobalt molybdate nano catalyst as high-performance supercapacitor. Ceram. Int. **44**, 17735–17742 (2018). https://doi.org/10.1016/j.ceramint.2018.06.240
34. T. Chen, S.Z. Li, L. Ma, X.Z. Zhao, G.J. Fang, Aldehyde reduced Co_3O_4 to form oxygen vacancy and enhance the electrochemical performance for oxygen evolution reaction and supercapacitors. Nanotechnology, 30 (2019) https://doi.org/10.1088/1361?6528/ab2a83
35. H. Bigdeli, M. Moradi, S. Hajati, M.A. Kiani, J. Toth, Cobalt terephthalate MOF-templated synthesis of porous nano-crystalline Co_3O_4 by the new indirect solid state thermolysis as cathode material of asymmetric supercapacitor. Phys. E-Low-Dimensional Syst. Nanostruct. **94**, 158–166 (2017). https://doi.org/10.1016/j.physe.2017.08.005
36. D. Guo, X. Song, F. Li, L. Tan, H. Ma, L. Zhang, Y. Zhao, Oriented synthesis of Co_3O_4 core-shell microspheres for high-performance asymmetric supercapacitor. Colloids Surf., A **546**, 1–8 (2018). https://doi.org/10.1016/j.colsurfa.2018.02.072
37. W.G. Huang, A.T. Zhang, X.R. Li, J.M. Tian, L.J. Yue, L. Cui, R.K. Zheng, D. Wei, J.Q. Liu, Multilayer NiMn layered double hydroxide nanosheets covered porous Co_3O_4 nanowire arrays with hierarchical structure for high-performance supercapacitors. J. Power Sources, 440 (2019) https://doi.org/10.1016/j.jpowsour.2019.227123
38. G.H. Cheng, T.Y. Kou, J. Zhang, C.H. Si, H. Gao, Z.H. Zhang, O_2^{2}/O functionalized oxygen-deficient Co_3O_4 nanorods as high performance supercapacitor electrodes and electrocatalysts towards water splitting. Nano Energy **38**, 155–166 (2017). https://doi.org/10.1016/j.nanoen.2017.05.043